JOURNAL OF MATERIALS SCIENCE 24 (1989) 1025–1037

Sintering and crystallization phenomena in Silceram glass

H. S. KIM, R. D. RAWLINGS, P. S. ROGERS
Department of Materials, Imperial College, London SW7 2BP, UK

An investigation has been carried out on the feasibility of employing a $CaO–MgO–Al_2O_3–SiO_2$ glass–ceramic (known as Silceram) as a matrix for a fibre composite produced by a powder route. Some important properties of the parent glass, e.g. surface energy, viscosity, have been measured as well as the kinetics and structural aspects of the sintering and crystallization processes. It was found that the crystallization of the main phase, diopside, occurred from the surface of individual particles and internally with activation energies of 392 to 452 kJ mol^{-1} and 258 to 323 kJ mol^{-1} respectively. However, the surface crystallization was only dominant when the glass powder was fine ($< 38\,\mu m$). The work has demonstrated that this glass–ceramic shows promise as the matrix component of a composite because

(i) both sintering and crystallization may be achieved by a single stage heat treatment at relatively low temperatures of 900° C to 1000° C, because the glass powder can be compressed and sintered by viscous flow before crystallization commences, and

(ii) the resulting microstructure is fine, and in the case of the hot-pressed material there is negligible porosity.

1. Introduction

Currently there is considerable interest in ceramic matrix composites due to their potentially superior mechanical properties. In particular, ceramic matrix–fibre composites can exhibit much improved toughness compared to the monolithic matrix material. Oxide ceramics, non-oxide ceramics, glass and glass–ceramics are all under consideration as matrix materials, the choice of matrix depending on such factors as cost and required mechanical properties.

A number of production routes are available for composites including sintering. There are two possibilities for the production of a glass–ceramic matrix composite by cold pressing and sintering, namely the sintering of particulate glass–ceramic with appropriate fibres or the sintering of powdered parent–glass and fibres followed by a crystallization treatment. The latter technique is preferable as lower sintering temperatures are required. Furthermore, by careful choice of the glass composition, glass particle size, and the sintering conditions it is possible both to sinter and crystallize in a single operation. A third sintering method is hot pressing the glass/fibre mixture and again, ideally, the conditions would be selected to achieve both sintering and crystallization during pressing.

This paper reports the results of an investigation of the feasibility of using a $CaO–MgO–Al_2O_3–SiO_2$ glass–ceramic (known as Silceram) as the matrix for a fibre composite. Although information is available in the literature on the processing, structure and properties of cast Silceram [1, 2, 3], which has been shown to be inexpensive, erosion resistant and to have good room and intermediate temperature mechanical properties, the production of Silceram ceramics by sintering has not been reported previously. The main factors controlling the sintering and crystallization behaviour, namely viscosity, surface and internal crystallization, have been determined as well as the crystal structure and microstructure of the compacted matrix.

2. Experimental procedure

2.1. Preparation of powder and compacts

Silceram of composition by wt %: 52.8, SiO_2; 12.5, Al_2O_3; 20, CaO; 5.9, MgO; 4.6, Fe_2O_3; 2.8, Na_2O; and 0.8, Cr_2O_3 (designated SCR19–34) was used to make a glass by melting in a platinum crucible at 1450° C for 1 h and then cooling rapidly to room temperature by quenching the melt in water.

The glass powder was produced by first crushing the glass in a percussion mortar and then grinding the crushed glass in a Tema mill. The glass powder was sieved using a 400 mesh ($< 38\,\mu m$) sieve with flowing water. The wet powder was dried in an oven at 120° C for 24 h. The particle size distribution of the powder was subsequently determined using a laser diffraction method (Malvern 3600 particle size analyser).

Both cold and hot pressing were used to produce compacts; the prepared powders were cold pressed, without any binder, in a 16.0 mm diameter steel die at a pressure of 10 MPa. The green pellets were then heat treated at temperatures in the range 850° C to 970° C for 0, 0.5, 1, 2, and 3 h followed by air cooling to room temperature. The hot pressing was carried out in a graphite die of bore diameter 12.7 mm at a maximum pressure of 6.6 MPa and at temperatures in the range 920 to 1100° C.

0022–2461/89 $03.00 + .12

2.2. Differential thermal analysis and structure of compacts

Differential thermal analysis (DTA) was carried out in static air on 50 mg samples of bulk and particulate glass with alumina as the reference material. Three powders were studied;

(i) a fine grained powder (particle size of $< 38\,\mu m$),

(ii) a medium grained powder (particle size range 75 to $150\,\mu m$) and

(iii) a coarse grained powder (particle size range 180 to $300\,\mu m$). Runs were performed at four different heating rates in the range 5 to 20° C min^{-1} from room temperature up to a maximum of 1200° C

An X-ray diffractometer was used to determine the crystalline phases present in the compacts as a function of heat treatment schedule and in selected DTA specimens. The microstructures were studied by means of scanning electron microscopy. Specimens were prepared for microscopic examinations by diamond polishing to a $1\,\mu m$ finish, etching in a solution of 0.5% HF–10% HCl in H_2O for 5 sec, and then coating with gold.

2.3. Viscosity and thermal expansion measurements

The low temperature viscosity of the parent glass was quantified by the determination of the Littleton softening point (Mg), which corresponds to a viscosity of $10^{6.6}$ Pa. sec. The procedure followed was in accordance with ASTM C338–73 [4] which states that Mg is the temperature at which a uniform glass fibre 0.55 to 0.75 mm in diameter and 23.5 cm long elongates under its own weight at a rate of 1 mm per min when the upper 10 cm of its length is heated at a rate of 5°C min^{-1}.

The thermal expansion behaviour of the glass and the glass–ceramic were measured using a dilatometer consisting of a silica specimen support tube in which the specimen (5 × 5 × 5 mm) was placed, with a spring-mounted silica thrust rod against one face. The dilatometer softening point (10^{10} to 10^{11} Pa. sec [5] or $10^{10.3}$ Pa. sec [6]), the glass transition temperature ($10^{12.4}$ Pa. sec [5, 6]) and the thermal expansion coefficient were measured from the traces of change in length against temperature.

2.4. Surface tension/densification of glass

The surface tension of the glass was measured by means of the sessile-drop method. The apparatus consisted of a horizontal tube furnace with specimen carriage, a light source to illuminate the field of view fully and uniformly, and an observation photo-microscope. The photo-microscope was set in horizontal alignment with the furnace tube and was used to obtain photographs of the drop profile intermittently up to a temperature at which the specimen had spread evenly over the base. A heating rate of 8° C min^{-1} was used and the surface tension was calculated using the tables of Bashforth and Adams [7]. The dimensional changes (and hence the relative shrinkage/expansion rate) of the cold pressed pellet was determined by measuring its silhouette area from photographs taken through the hot stage microscope over a wide temperature range. Furthermore, the linear contraction of the cold pressed pellet (sample size 5 × 5 × 5 mm) under identical conditions was measured by using a dilatometer.

3. Results

3.1. Physical characterization of parent glass

The parent glass drop profiles at various temperatures in the range 30° C to 1260° C are presented in Fig. 1. The photograph at 1250° C shows that the hemisphere point, at which the test specimen has lost its original shape entirely, is no longer swollen and is fused down to a hemispherical mass. The contact angle at 1250° C was measured from the photograph and the surface energy calculated using the tables due to Bashforth and Adams; the surface energy so calculated was $510 \pm 20\,mJ\,m^{-2}$.

There was a slight drop in the DTA base-line at the glass transition temperature for both the bulk and the powdered samples (Fig. 2). Three values were taken from any given DTA plot to specify the transition temperature, namely T_{g_1}, which corresponded to the onset of the drop, T_{g_3} the temperature at the minimum in the base-line, and T_{g_2} the mean of T_{g_1} and T_{g_3}. These temperatures are given in Table I. The slower the heating rate (β) the smaller the magnitude of the drop and in the case of the slowest rate of 5° C min^{-1} the discontinuity in the base line was too small to accurately determine T_{g_1} and T_{g_3}; glass transition temperature values for this heating rate are therefore not given in Table I. Moynihan, Easteal and Wilder [8] found that the heating rate dependence of the glass transition temperature T_g follows an Arrhenius-type rate equation:

$$\beta = C \exp(-E_g/RT_g) \quad (1)$$

TABLE I Relationship between heating rate and glass transition temperature (T_g) from differential thermal analysis (DTA) and Dilatometry (D). See text for definition of T_{g_1}, T_{g_2} etc.

Sample	Method	T_g (°C)	Heating rate (° C min^{-1})			E_g (kJ mol^{-1})
			10	15	20	
Powder glass	DTA	T_{g_3}	738	744	750	502
Bulk glass	DTA	T_{g_1}	703	705	708	969
	DTA	T_{g_2}	716	720	724	727
	DTA	T_{g_3}	730	735	740	582
	D	T_{g_0}	702			
	D	T_{g_f}	759			
Silceram	D	T_{g_0}	710			
Bulk	D	T_{g_f}	768			
						Mean 695 ± 178

where β is the heating rate, C a constant, R the universal gas constant, and E_g is the activation enthalpy for the rate-controlling relaxation process. The present data yielded linear relationships between log (β) and $1/T_g$ in accordance with Equation 1 (Fig. 3). The values for E_g calculated from the slopes are tabulated in Table I. The E_g values varied according to the definition of T_g and hence the mean E_g value is also given in Table I. It is not clear whether this variation has any physical basis or just reflects experimental scatter, as a slight error in the determination of a given T_g value has a considerable effect on the calculated E_g because T_g only changes by about 10° C over the range of heating rates employed.

An increase in the slope of the dilatometric plots of linear thermal expansion against temperature for the parent glass and the Silceram glass-ceramic was observed during the glass transition (Fig. 4). The temperatures at the onset and end of the region of increased slope are designated as T_{g_0} and T_{g_f} respectively and are presented in Table I together with the T_g values from the DTA. It can be seen that there is good agreement between T_{g_0} and T_{g_1}, but that T_{g_f} is greater than T_{g_3}.

The coefficient of thermal expansion (α) over the temperature range 100° C up to the glass transition was determined from the dilatometric plots, which were linear over this temperature range. The values obtained were $6.0 \times 10^{-6}\,K^{-1}$ and $7.5 \times 10^{-6}\,K^{-1}$ for the parent glass and the glass-ceramic respectively.

The low temperature viscosity (η) data determined from the Littleton softening point and by dilatometry were combined with the previously reported values at temperatures above 1200° C [9] to produce the plot of viscosity against temperature shown in Fig. 5. The viscosity at the hemispherical profile temperature of 1250° C is just over 10 Pa. sec which is within the range specified [29] for the melting temperature of a glass. The curves for alumino-silicate glass, soda-lime glass [24] and shale glass [26] are also shown in Fig. 5 and it can be seen that these have a similar form to that for the parent Silceram glass. The data for the parent glass were fitted to the Vogel-Fulcher-Tammann (VFT) equation:

$$\log \eta = A + B/(T - T_0) \qquad (2)$$

where A, B and T_0 are empirical constants. The constants A, B and T_0 were calculated, by a least squares fit over the complete temperature range of the investigation, to be -3.35, 5090 and 401° C respectively.

Alternatively, the temperature dependence of the reciprocal viscosity may be considered to obey a relationship of the form of Equation 1 with the important parameter being the activation energy for viscous flow (E_η). Plots of log (η) versus $1/T$ for the parent glass exhibited a change in slope and hence two values for E_η were calculated. The activation energy for viscous flow decreases with increasing temperature; at low temperature E_η was $630\,kJ\,mol^{-1}$ whereas a lower value of $184\,kJ\,mol^{-1}$ was applicable at the higher temperatures. The transition, obtained by extrapolation, between the two temperature regions occurred at approximately 1060° C.

3.2. Sintering and crystallization

The effect of particle size of the glass powders on crystallization was monitored by DTA. As shown in Fig. 6a, the crystallization of coarse powders and bulk glass was associated with a single exothermic peak at a temperature of about 962° C for a $10°\,C\,min^{-1}$ heating rate. In contrast, two exothermic peaks at temperatures of about 922° C and 960° C (Fig. 6b) accompanied the crystallization of the fine powder ($< 38\,\mu m$ particle size).

Irrespective of the glass powder particle size, the exothermic peak(s) shifted to higher temperatures

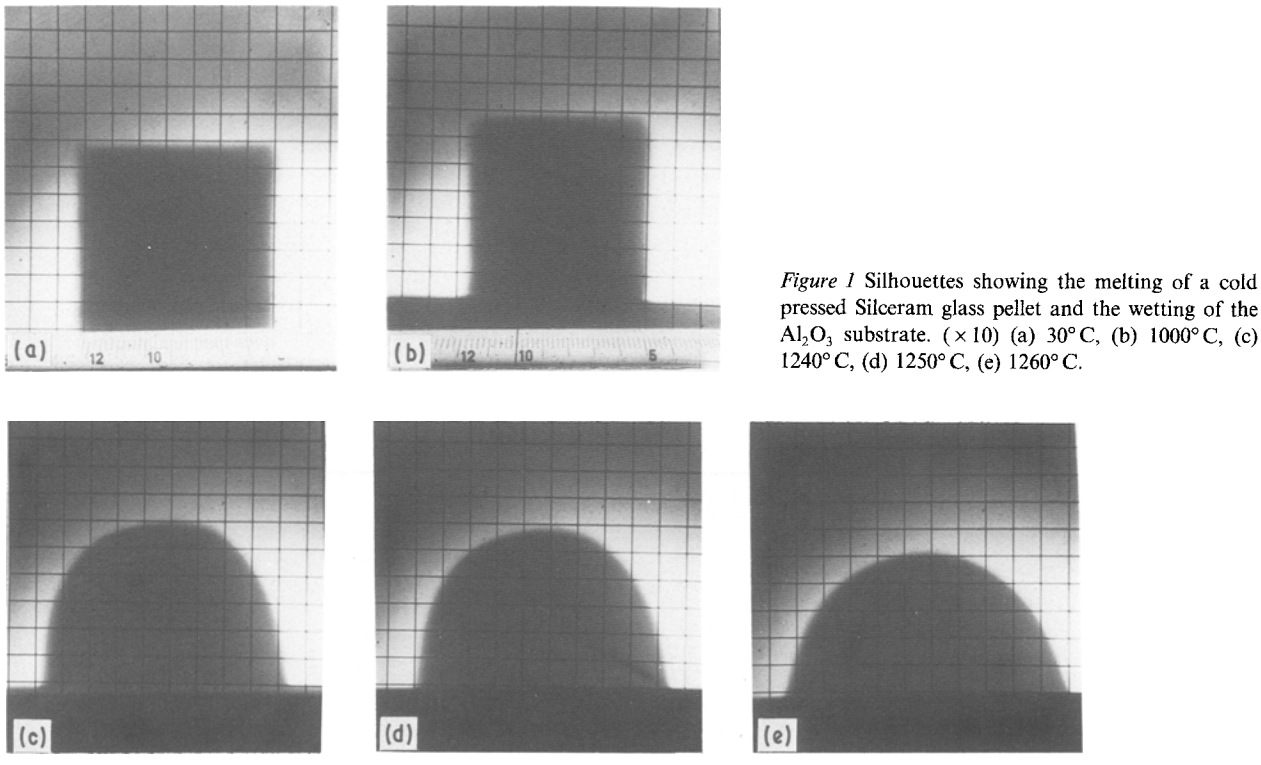

Figure 1 Silhouettes showing the melting of a cold pressed Silceram glass pellet and the wetting of the Al_2O_3 substrate. (×10) (a) 30° C, (b) 1000° C, (c) 1240° C, (d) 1250° C, (e) 1260° C.

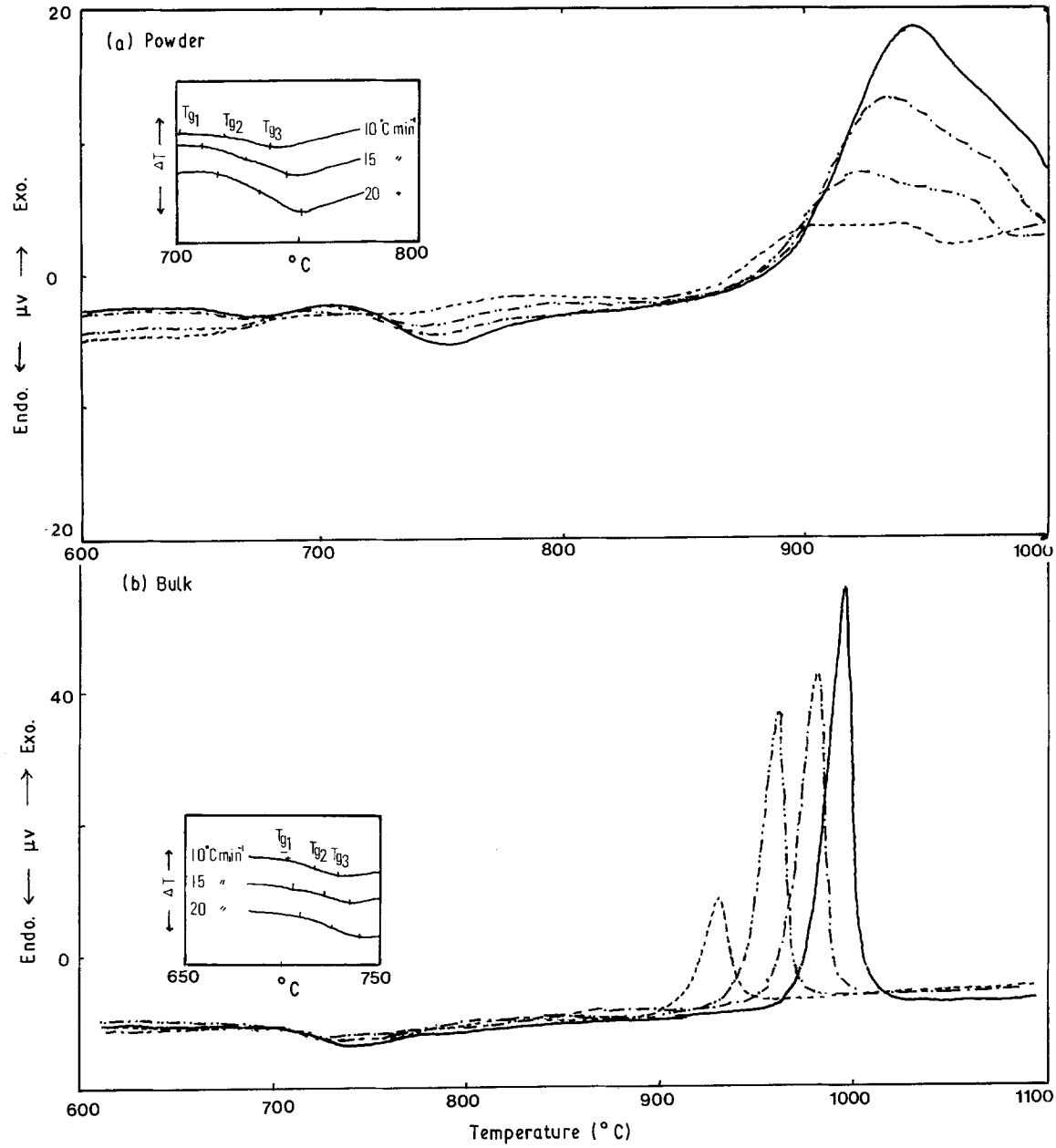

Figure 2 DTA curves for powdered and bulk Silceram glass samples as a function of heating rate showing a drop in the base line at the glass transition and an exothermic peak at higher temperature. (a) Powder glass, (b) Bulk glass. (– – –) 5° C min^{-1}, (–·–·–·–) 10° C min^{-1}, (–·–·–) 15° C min^{-1}, (——) 20° C min^{-1}.

with increasing heating rate (Fig. 2). The relationship between heating rate (β) and peak temperature (T_p) for bulk and fine powder samples is summarized in Table II. The activation energy for crystallization and the Avrami exponent from the Johnson–Mehl–Avrami equation were calculated by means of the Marotta method [10], from plots of log (β) against $1/T_p$ (Fig. 7) and log (ΔT) against $1/T$ (Fig. 8) respectively. These values, together with values for the activation energy obtained by the analyses due to Kissinger [11] and Augis–Bennett [12], are presented in Table III. In view of these results additional DTA experiments were carried out on a parent glass which did not contain the Cr_2O_3 nucleating agent. The results for this material are also given in Table III.

Typical microstructures from specimens prepared by cold pressing and heating are shown in Fig. 9. Surface nucleation and crystal growth always occurred, but, in general, did not prevent internal crystallization (see Fig. 9b and d). However, it was observed that

TABLE II The relationship between heating rate (β) and peak temperature (T_p)

Heating rate β (° C min^{-1})	Bulk sample	Fine powder		Fine powder (without Cr_2O_3)
	T_p (° C)	1st T_p (° C)	2nd T_p (° C)	T_p (° C)
5	931	902	938	955
10	962	922	960	975
15	981	932	979	–
20	996	944	990	995

TABLE III Activation energy and Avrami exponent derived from various non-isothermal DTA methods

Material	Activation energy ($kJ\,mol^{-1}$)				Arami exponent
	Marotta	Kissinger	Augis–Bennett	Average value	n value
Bulk glass	268	251	255	258	4.1
Powder glass					
1st peak	402	385	389	392	1.1
2nd peak	339	314	318	323	–
Powder glass w/o* Cr_2O_3	473	439	444	452	1.1

*w/o Without.

internal crystallization occurred more readily in the larger particles (Figs 9b and 10); furthermore the internal crystals tended to form in the central region of the particles with the result that, after certain heat treatments, a ring of residual glass separated these crystals from the surface nucleated crystals. This boundary region between the surface crystallization and the crystals formed internally probably results from the increased stability to crystallization which follows changes in composition of the glass as crystallization occurs. After long heat treatments, particularly at high temperatures, an additional crystalline phase was detected, which was more angular and had a larger aspect ratio than the primary crystal phase.

The hot pressed material also consisted of surface and internally nucleated crystals. The internal crystals were larger than the surface crystals (Figs 11a and b) but the mean crystal size was less than that found in monolithic, cast Silceram, (Fig. 11d). Due to flattening of the particles during hot pressing some layering of the microstructure could be discerned in sections parallel to the pressing axis, i.e. the regions of residual glass and surface crystallization were elongated perpendicular to the pressing axis (Fig. 11b). The angular phase observed in some of the sintered cold pressed samples was also detected in the material hot pressed at the higher temperatures (Fig. 12).

X-ray diffraction demonstrated that the primary crystalline phase in the cold pressed and sintered samples and in the hot pressed material were diopside. The angular crystals formed under certain conditions were shown to be anorthite. Diopside is the crystalline phase in cast Silceram, and anorthite is only observed after long heat treatments [9]. In order to document the kinetics of anorthite formation during sintering of green pellets, the ratio (R_i) of the intensity of the X-ray peak at $2\theta = 22.1°$ for anorthite to that of the nearby peak at $2\theta = 20.0°$ for diopside was determined over a range of heat treatment times and temperatures. Neither the volume fraction of anorthite corresponding to a given R_i value nor the equilibrium volume fraction of anorthite is known, nevertheless a pseudo time–temperature–transformation diagram was produced by plotting curves of constant R_i (Fig. 13). This diagram clearly shows that anorthite forms rapidly at temperatures around 950° C but that the rate of formation is very slow at temperatures below 900° C. The higher temperature required for the formation of anorthite compared with that required for diopside in Silceram is consistent with the kinetics of crystallization of these phases from their own parent glasses, e.g. the temperature has to be 50 to 100° C higher for anorthite to achieve the same growth rate as diopside [13, 14].

The results of the hot stage microscopy experiments which were carried out to follow the changes in volume associated with both the sintering and crystallization of the powders are given in Fig. 14. The relative densification in this figure is defined as $(A_0 - A_T)/A_0$, where A_0 and A_T are the initial area of the silhouette and its area at temperature T respectively. The figure shows that the densification rate is greatest over the

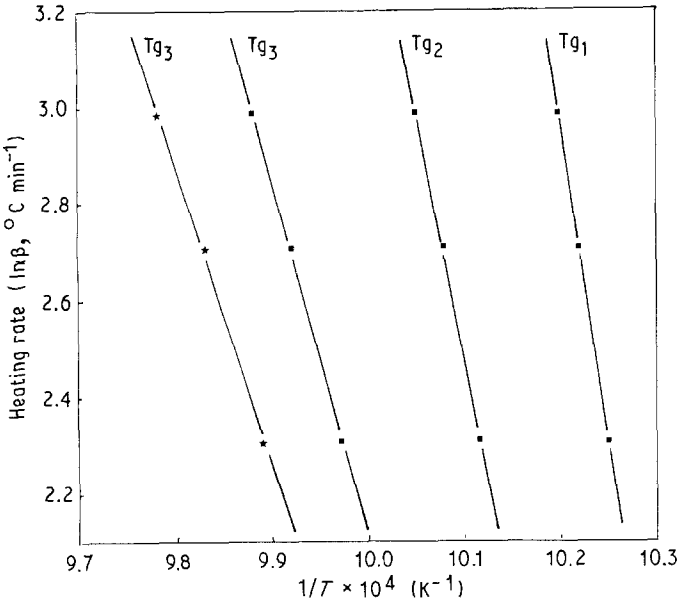

Figure 3 Determination of the activation energy for viscous flow using Arrhenius type plot of reciprocal of the glass transition temperature (T_{g_1}, T_{g_2}, T_{g_3}) against heating rate (β) for (■) bulk and (★) powdered Silceram parent glass.

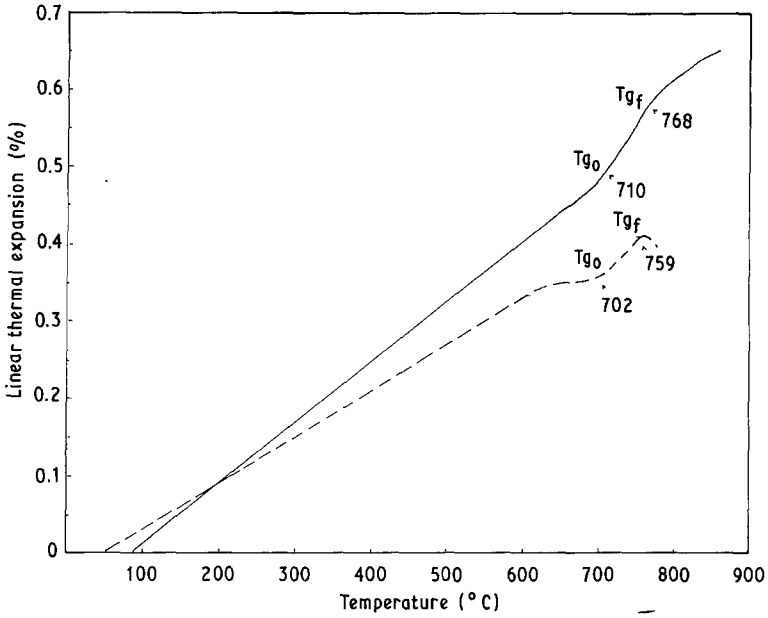

Figure 4 Thermal expansion against temperature for (——) crystallized bulk Silceram and (– – –) quenched glass (Heating rate 10° C min^{-1}).

temperature range 800° C to 850° C. Regarding the densification of glass, the linear contraction and the relative change of area show a similar behaviour with increasing temperature, as shown in Fig. 14. The microstructure of pellets at 820, 900 and 980° C show a change in pore shape (Fig. 15). The irregular pore shape at the initial stage of solid state sintering (Fig. 15a) gives way to isolated spherical pores due to viscous flow during the final stages of sintering (Fig. 15b), and lastly the pores expanded and became more angular due to the volume changes associated with crystallization (Fig. 15c).

4. Discussion

Barrett and Thomas have reported that the surface energy of melts in the $CaO–Al_2O_3–SiO_2$ system increases with increasing alumina and silica content [15]. The melt nearest to the composition of Silceram parent glass investigated by these workers was 25% CaO–20% Al_2O_3–55% SiO_2 and had a surface energy of about 440 mJ m^{-2} at 1400° C, which is consistent with the value determined in this study of 510 ± 20 mJ m^{-2} at 1250° C. These values are higher than those of many other glasses, e.g. soda–lime–silica 315 mJ m^{-2}, lead disilicate 210 mJ m^{-2} and silica 290 mJ m^{-2}. Sintering occurs because of the reduction in free energy associated with the replacement of solid–gas interfaces with lower energy solid–solid interfaces. Given the high surface energy of the Silceram parent glass, it therefore follows that there is a large thermodynamic driving force for sintering.

The good fit of the viscosity data over the temperature range 700 to 1450° C to the VFT equation yielded a value of T_0 of 401° C. This is lower than expected; previous workers [16, 17] have found that T_0 was about 50° C higher than T_g, whereas T_g for Silceram parent glass has been shown to be in excess of 700° C. Furthermore, Gutzow [18] has proposed that for typical glass forming melts T_0 is of the order of one

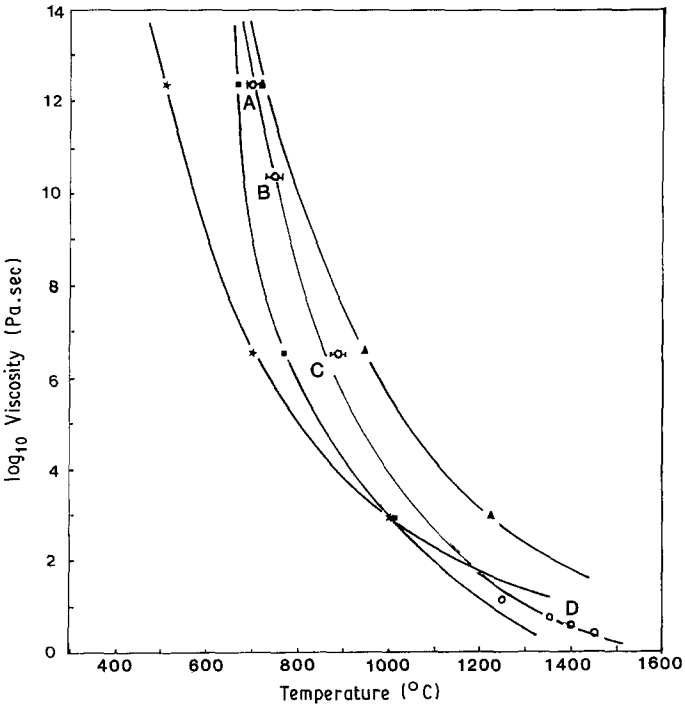

Figure 5 Comparison of the temperature dependence of the viscosity of Silceram parent glass with that of other glasses. Experimental points; *A* and *B* were determined by dilatometry, *C* by fibre elongation method and *D* by falling sphere method [9]. The curve for the parent glass is calculated from the Vogel–Fulcher–Tammann equation. (▲) Alumino-silicate, (★) Soda-lime glass [24], (■) Shale glass [26] and (○) Silceram glass.

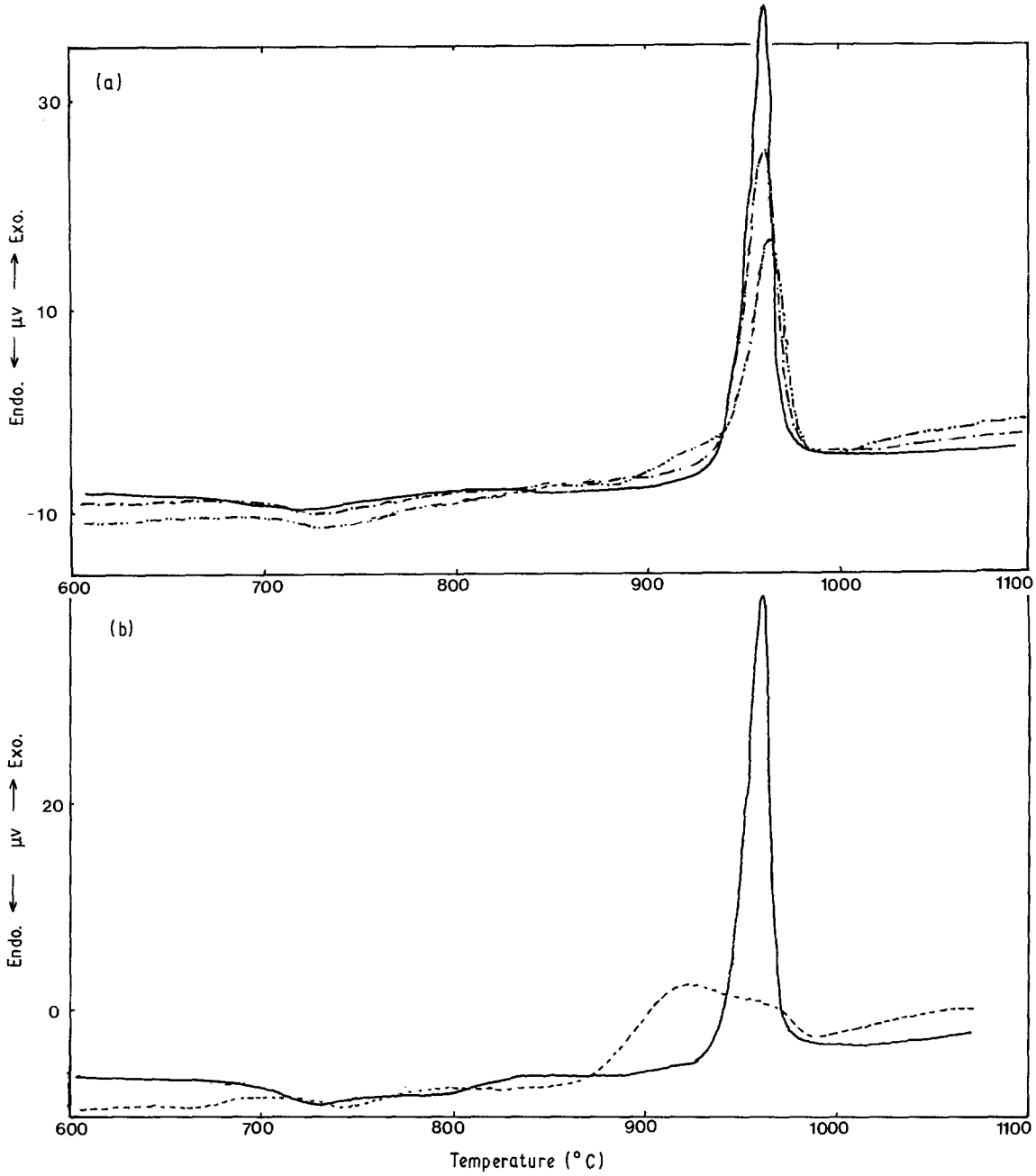

Figure 6 Effect of particle size on the DTA curves of powdered Silceram parent glass (heating rate 10° C min^{-1}). (a) Coarse powder, (— · · · —) 75 to 150 μm, (— · — · —) 180 to 300 μm, (——) Bulk. (b) Fine powder, (— — —) < 38 μm, (——) Bulk.

half to two thirds of the melting point. The liquidus of the parent glass is in the region of 1250° C, thus this criterion also predicts a T_0 value much greater than that calculated. As the constants A and B of Equation 2 are not anomalous, e.g. soda-lime-silica glass has similar A and B values of approximately -2 and 5000, respectively, the consequence of the low T_0 value is that the viscosity of the Silceram parent glass at a given temperature is lower than might be estimated from the glass transition or melting temperatures. This should facilitate sintering.

The activation energy for viscous flow E_η was 630 kJ mol^{-1} at temperatures below 1060° C but fell to 184 kJ mol^{-1} at higher temperatures. A factor which may account for at least a part of this fall in E_η at high temperatures is a change in the liquid structure, the structure becoming more open as the temperature rises. The low temperature E_η can be compared with the data obtained for the CaO–MgO–Al_2O_3–SiO_2 system as a function of the Fe^{2+} and Fe^{3+} contents (Williamson *et al.* [19]). They reported E_η values at 910° C of 440 kJ mol^{-1} and 650 kJ mol^{-1} for glasses with 13% and 70% of the iron as Fe^{2+}. According to Carter [20] the Fe^{2+} content as a percentage of the total number of Fe ions in Silceram parent glass is 26.8%, therefore E_η for this glass is slightly higher than, but of a similar order to, the previously published values for related glasses.

The mean value for the activation energy (E_g) of 695 $\pm$ 178 kJ mol^{-1} calculated from the glass transition temperature measurements is in agreement with the low temperature value for E_η. This suggests that the same rate-controlling molecular processes are involved in the glass transition and in low temperature viscous flow.

The thermal expansion coefficient of a glass-ceramic depends on the volume fraction, elastic properties and the coefficients of thermal expansion of the constituent vitreous and crystalline phases. It has been proposed [21] that the coefficient of thermal

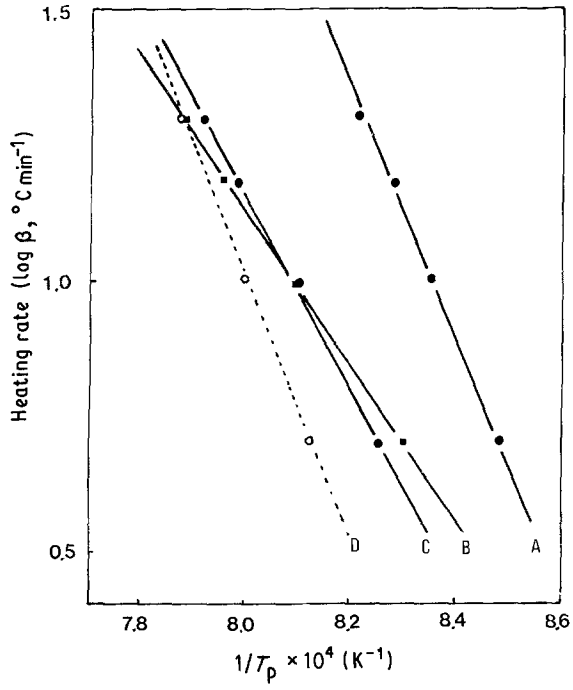

Figure 7 Determination of the activation energy from the relationship between heating rate (β) and reciprocal of absolute exothermic peak temperature ($1/T_p$). (A) Powder glass ($< 38\,\mu m$); 1st peak, (B) bulk glass, (C) powder glass ($< 38\,\mu m$); 2nd peak, (D) powder glass without Cr_2O_3.

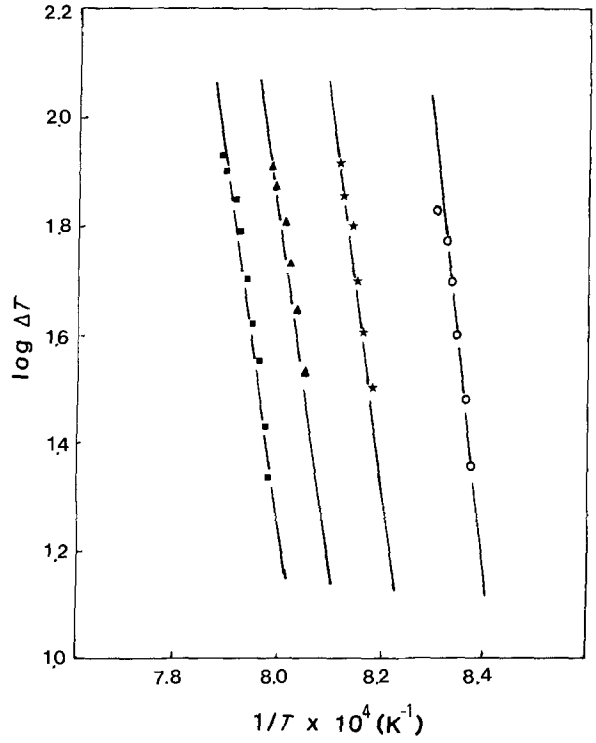

Figure 8 Determination of the Avrami exponent n for glass powder using the method due to Marotta [10]. (○) 5° C min^{-1}, (★) 10° C min^{-1}, (▲) 15° C min^{-1}, (■) 20° C min^{-1}.

expansion, α, of a glass–ceramic is given by the expression originally obtained by Turner [22]:

$$\alpha = (\alpha_1 K_1 V_1 + \alpha_2 K_2 V_2 + \cdots)/(K_1 V_1 + K_2 V_2 + \cdots) \quad (3)$$

where α_i, K_i and V_i are the volume expansion coefficient, bulk modulus and volume fraction of phase i respectively. The value calculated for Silceram from Equation 3 using V_i and α (glass) from the present work, together with values from the literature for the other parameters ($K_{diopside}$ [23], K_{glass} [24] and $\alpha_{diopside}$ [25]), was $7.4 \times 10^{-6}\,°C^{-1}$. This corresponds well to the experimentally determined value, hence in further development work on these materials Equation 3 may be used with some confidence in estimations of thermal

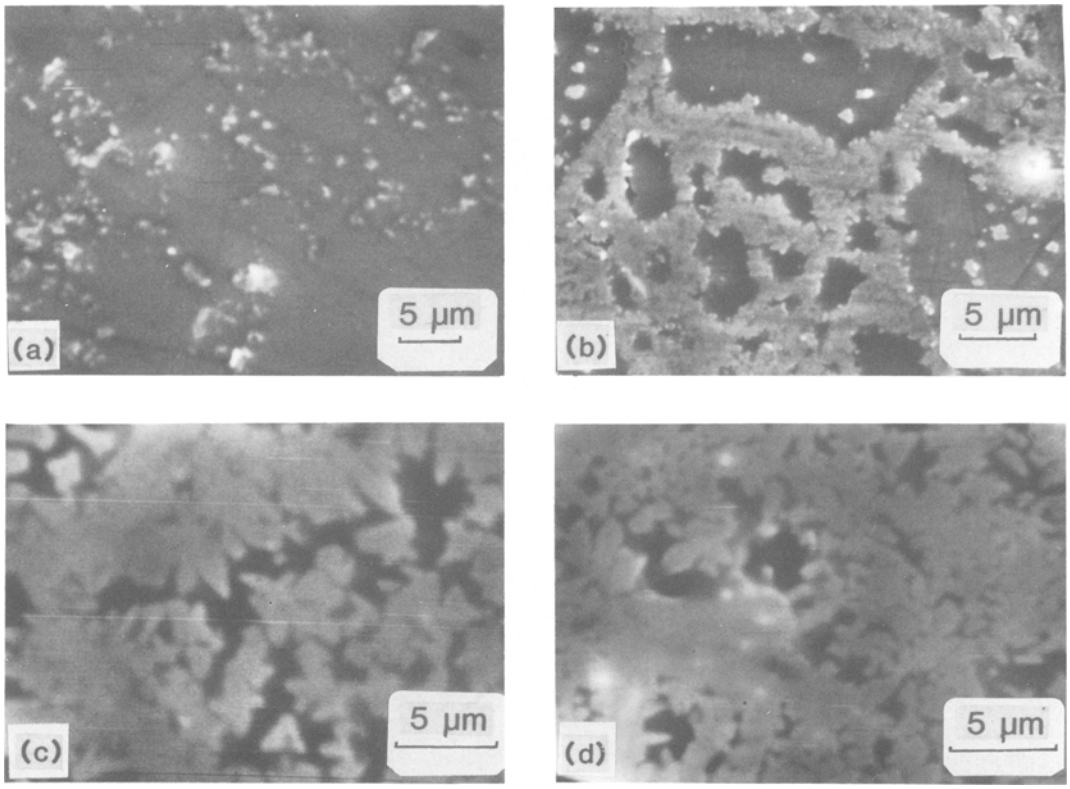

Figure 9 Scanning electron micrographs of cold-pressed material after the following heat treatments: (a) 800° C for 2 h, (b) 850° C for 2 h, (c) 920° C for 30 min, and (d) 970° C for 30 min.

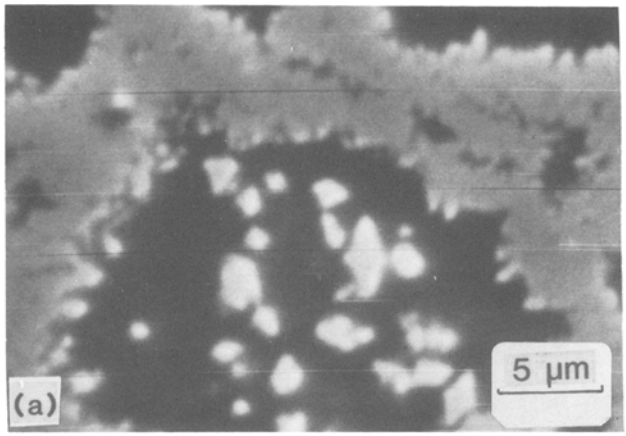

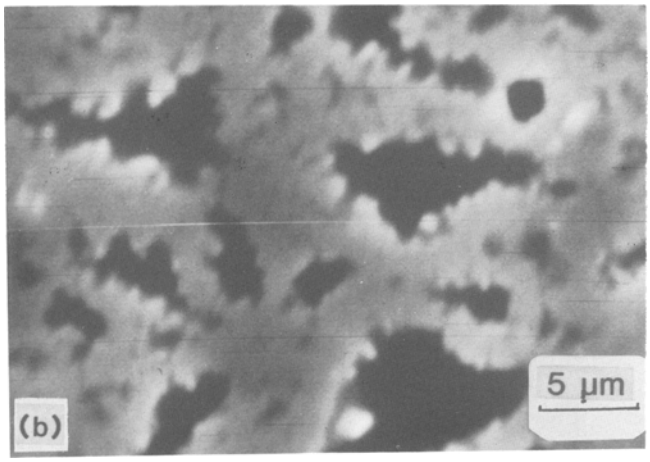

Figure 10 Scanning electron micrographs showing that internal crystallization occurred more readily in larger particles: (a) large particles, (b) small particles.

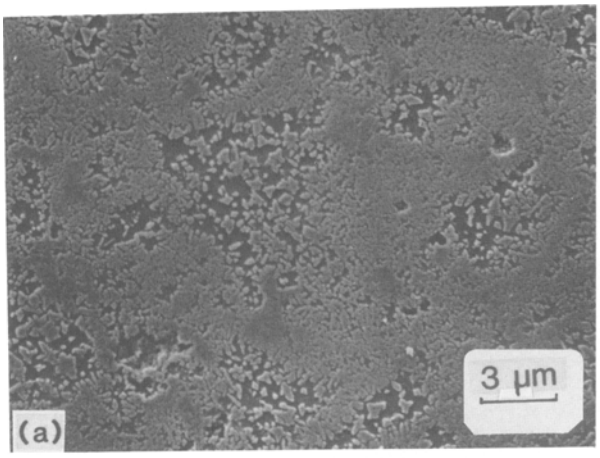

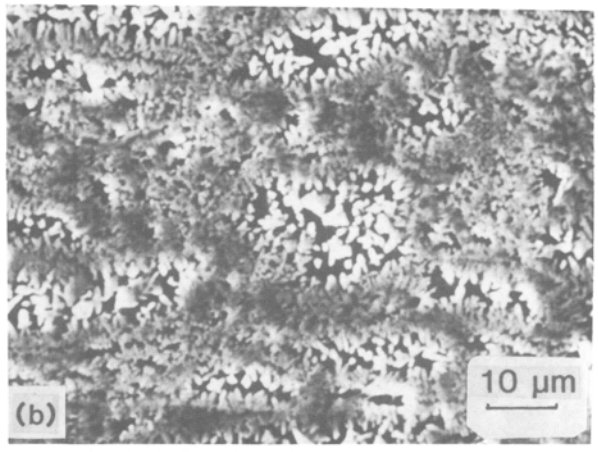

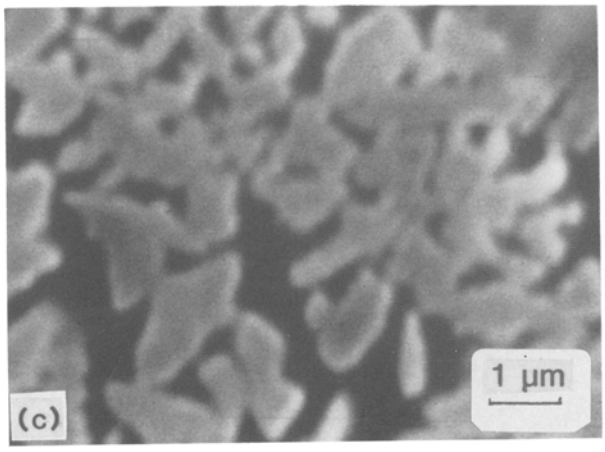

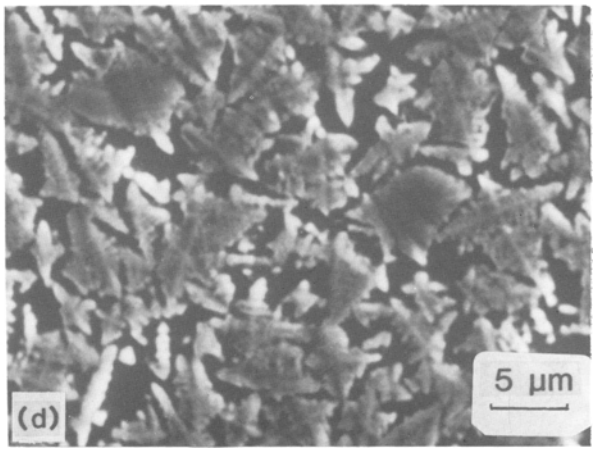

Figure 11 Scanning electron micrographs of: (a) hot pressed (950° C, 3 h, 6.6 MPa) section normal to axis of pressing, (b) hot pressed (850° C, 1 h; 950° C, 1 h, 6.6 MPa) section parallel to axis of pressing, (c) hot pressed (950° C, 3 h, 6.6 MPa), (d) cast Silceram.

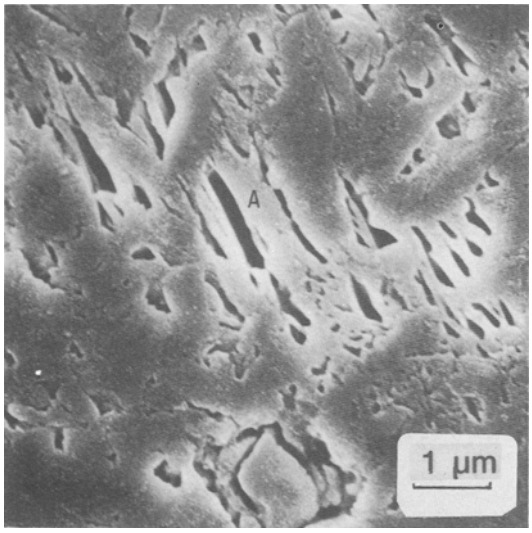

Figure 12 Scanning electron micrograph of a hot pressed sample of 1000° C for 3 h at 6.6 MPa showing the angular crystals of anorthite.

expansion behaviour. A knowledge of the thermal expansion coefficients of both the matrix and the fibre is important in composite technology because a difference in the thermal expansivities results in residual stresses as the composite cools down from the heat treatment temperature. For example, the coefficient of thermal expansion of Nicalon SiC fibre is $3.1 \times 10^{-6}\,°C^{-1}$ [28], therefore if these fibres were incorporated in a Silceram matrix there would be a tendency for tensile stresses to be set up in the matrix.

For glasses in which surface nucleation predominates, the temperature of the exothermic crystallization peak is strongly dependent on the surface area of the powder. In such cases, the finer the powder the lower the temperature of the peak. In contrast, in a glass with sufficient nuclei for internal crystallization, powder size will have little effect on the peak temperature. Thus the single exothermic peak at around 960° C observed (Fig. 6) for the bulk glass and the coarse (> 75 μm) powders at the $10°\,C\,min^{-1}$ heating rate is indicative of the domination of internal crystallization. However, for the very fine powder the increasing propensity for surface crystallization results in the two overlapping peaks shown in Figs 2a and 6b. The lower temperature peak is attributed to surface crystallization and the second peak to internal crystallization. The agreement between the temperatures of the second peak of the fine powder and the single peak of the bulk/coarse powder specimens is consistent with this interpretation of these peaks (Table II).

Additional support for these proposals may be obtained from the activation energy, and Avrami exponent, n, values of Table III. The activation energy for internal crystallization determined from the bulk sample ($258\,kJ\,mol^{-1}$) is of the same order as that calculated from the second peak ($323\,kJ\,mol^{-1}$). Furthermore, the Avrami exponent for the bulk sample of 4.1 is consistent with the three-dimensional crystal growth observed by microscopy together with an increasing number of nuclei during the crystallization process.

The Cr_2O_3-free bulk sample was tested in order to obtain solely surface crystallization. Although the activation energy of $452\,kJ\,mol^{-1}$ from this sample is greater than that determined from the first peak from the fine powder ($392\,kJ\,mol^{-1}$), the two values are considered close enough to confirm the assignation of the peaks. The corresponding n values from these peaks were identical, namely 1.1: this value, which is close to unity, is indicative of one-dimensional growth, as experimentally observed for surface crystallization, from a constant number of nucleation sites. Finally, microscopical evidence from DTA runs stopped at various temperatures around the exothermic peaks of the fine powder confirmed that surface crystallization occurred at the first peak and internal crystallization at the second.

The activation energy for surface crystallization, E_s, is well within the range of experimental values reported for the $CaO–MgO–Al_2O_3–SiO_2$ system with iron oxide additions, namely 335 to $418\,kJ\,mol^{-1}$ for Fe^{2+} contents between 26 and 35% [19]. E_s is greater than the activation energy for internal crystallization E_b; a similar difference in E_s and E_b has been observed for a shale glass with Cr_2O_3 as a nucleating agent

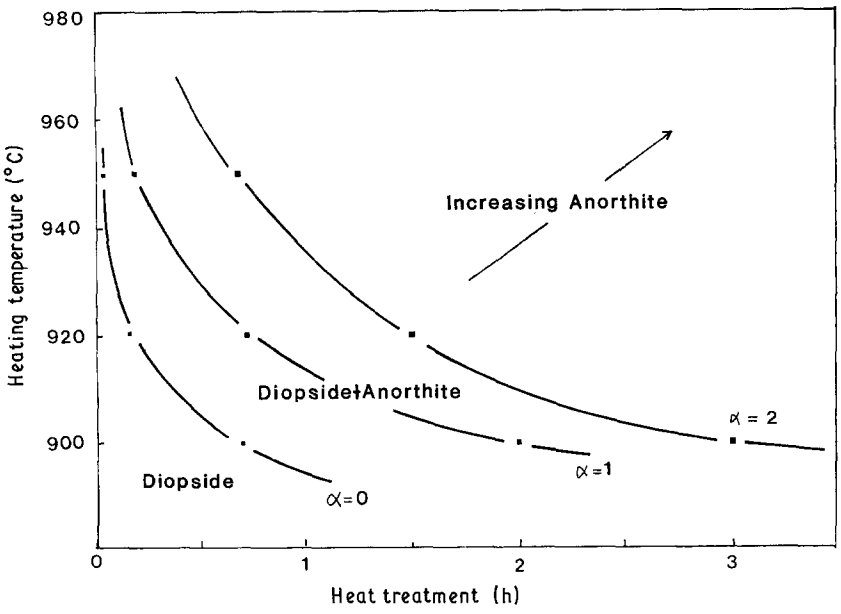

Figure 13 Isothermal transformation plot for sintered Silceram glass–ceramic constructed from X-ray data. ($\alpha = I_{20=22.1}/I_{20=20.0}$).

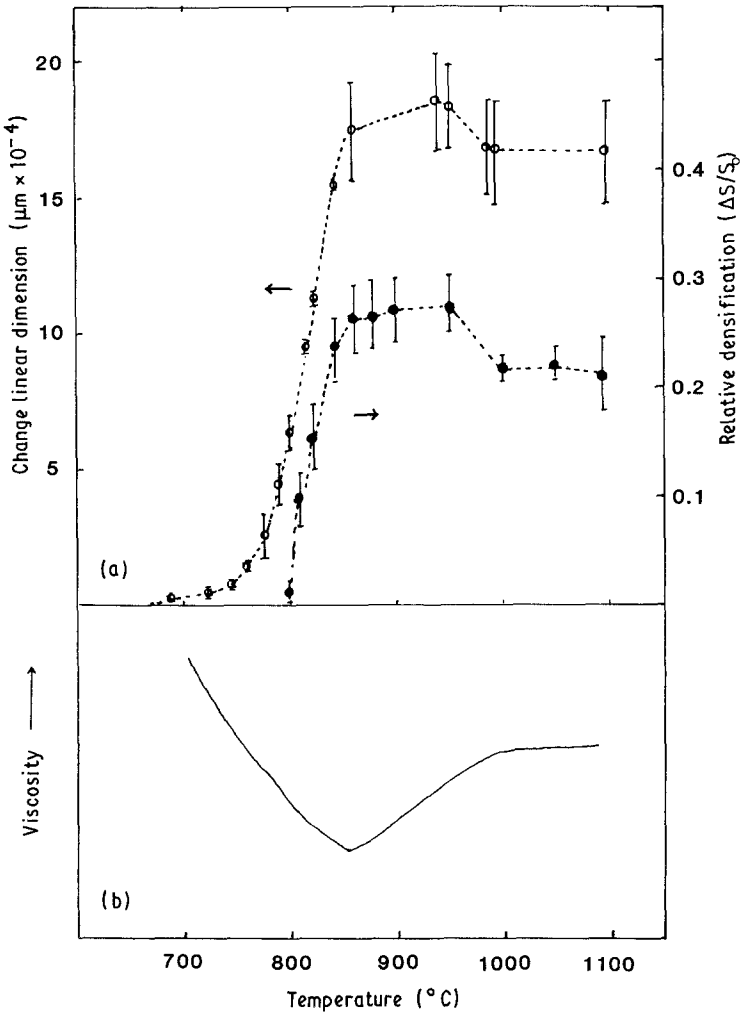

Figure 14 (a) Changes in linear dimension (dilatometry) and relative densification $(A_0 - A_1)/A_0$ (silhouette) over a wide temperature range. (b) Schematic relationship between viscosity and temperature for the sintered glass–ceramic.

where the reported values were 415 and 243 kJ mol^{-1} for E_s and E_b respectively [26]. This difference in E_s and E_b could be accounted for by the surface-nucleated phase being different from the phase which crystallizes internally. However, X-ray diffraction of specimens from DTA runs interrupted at 930° C (powder) and 980° C (powder and bulk specimens) showed only diopside to be present. Note that, in accordance with Fig. 13, the times in the DTA apparatus at these temperatures are insufficient for the formation of anorthite. An explanation based on differences in crystallographic orientation and/or growth geometry would appear to be more appropriate. The surface-nucleated crystals are aligned with a growth direction perpendicular to the surface and the specific reorientation of the molecules from the glass to the surface crystalline phase will therefore require a greater activation energy than that for the corresponding process from glass to the randomly orientated internal crystals. The effect on the activation energies of surface growth being one-dimensional and internal crystal growth three-dimensional has been studied by Matusita, Sakka and Matsui [27]. They showed that as a consequence of the geometries of surface and internal crystallization the activation energy of the former could be three times that of the latter, although this should probably be taken as an upper limit.

It is clear from the DTA data and the microscopy that only for the finest powder investigated is surface crystallization dominant. Thus by choice of powder size it will be possible to vary the proportions of internally and surface nucleated crystals in a sintered Silceram matrix. At this stage the relationship between the proportions and mechanical behaviour of the sintered material is unknown, but the properties are expected to be superior to those of cast Silceram because the crystallites, whether internally or surface nucleated, are finer than the dendritic crystals in the cast material. Furthermore, the increased propensity for the formation of anorthite in the sintered material gives another controllable feature that may be beneficial in certain situations.

This work has demonstrated that powdered Silceram parent glass may be cold pressed and heat treated or hot pressed so that the sintering and crystallization processes overlap. The various stages of densification (Fig. 14a) may be correlated with a schematic viscosity curve (Fig. 14b) constructed from viscosity and crystallization data. Sintering commences at about 800° C and densification occurs at a rapid rate at temperature up to 850° C as the viscosity of the glass is low (Fig. 14a). Surface crystallization starts at about 850° C and results in a reduction in the densification rate and an increase in viscosity (Fig. 14b). The onset of internal crystallization at 880° C further decreases the densification rate and increases the viscosity. The slight increase in dimensions observed over temperature range 940–990° C is attributed to the pore expansion caused by crystallization as shown in Fig. 15c.

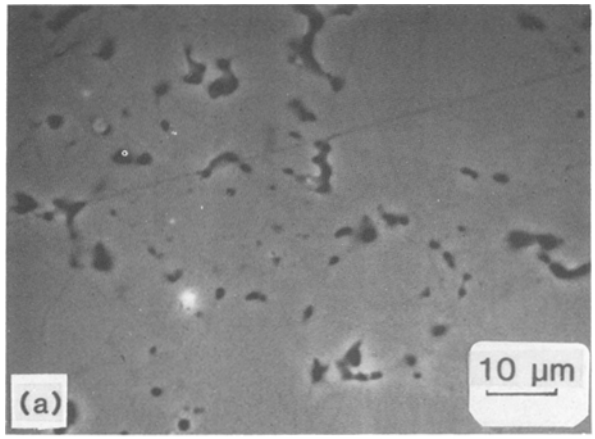

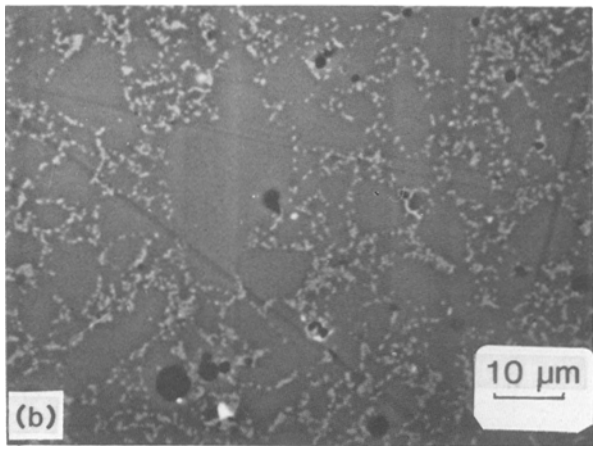

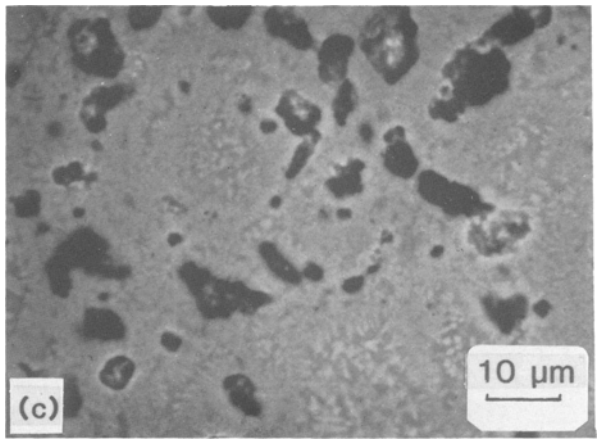

Figure 15 Scanning electron micrographs of a cold pressed sample showing the pore morphology at: (a) 820° C, (b) 900° C, (c) 980° C.

5. Conclusions

1. The surface energy was determined at 1250° C from the hemispherical condition using the sessile drop technique and found to be $510 \pm 20\,mJ\,m^{-2}$.

2. The glass transition temperature of parent glass varied with heating rate but was in the range 700 to 760° C. The heating rate dependence followed an Arrhenius equation with a mean activation energy of $695 \pm 178\,kJ\,mol^{-1}$.

3. The temperature dependence of the viscosity of the parent glass fitted the Vogel–Fulcher–Tammann equation over the temperature range 700 to 1450° C. Analysis in terms of activation energies yielded a value of $630\,kJ\,mol^{-1}$ below 1060° C and $184\,kJ\,mol^{-1}$ at higher temperatures.

4. The coefficient of thermal expansion of Silceram glass–ceramic was $7.5 \times 10^{-6}\,K^{-1}$. This value was in good agreement with that calculated from the volume fractions and elastic/thermal properties of the constituent phases glass and diopside, namely $7.4 \times 10^{-6}\,K^{-1}$.

5. The main crystalline phase grew from both surface and internal nuclei. The activation energy for surface crystallization was 392 to $452\,kJ\,mol^{-1}$ and that for internal crystallization 258 to $323\,kJ\,mol^{-1}$. The Avrami exponents for surface and internal crystallization were 1.1 and 4.1 respectively.

6. Surface crystallization was only dominant in the finest powder investigated. For all powders the internally nucleated crystals were larger than those nucleated at the surface, but nevertheless the microstructure of sintered Silceram was finer than that of the cast material.

7. Anorthite was observed in some hot pressed and heat treated cold pressed samples. Anorthite formed more readily in powdered samples than in cast Silceram and its time–temperature–transformation curve was displaced to higher temperatures with respect to diopside.

8. It was demonstrated that sintering and crystallization of the parent glass may be achieved during a single stage heat treatment of green pellets or by hot pressing.

9. The work has established that glass–ceramics of this composition show promise as the matrix component for composite materials, particularly if hot pressed.

Acknowledgements

The authors would like to thank Drs S. Carter, J. F. Bell and C. B. Ponton for discussions and Miss M. Campbell for her permission to publish viscosity data (Fig. 5). The authors gratefully acknowledge POSCO Scholarship Society for financial support to HSK and Professor D. W. Pashley FRS for the provision of research facilities.

References

1. P. S. ROGERS, J. WILLIAMSON, J. F. BELL and M. CAMPBELL, in "Energy Conservation in Industry – Applications and Techniques", edited by A. S. Strub and H. Ehringer (VDI, Verlag, Dusseldorf, 1984) p. 280.
2. S. CARTER, C. B. PONTON, R. D. RAWLINGS and P. S. ROGERS, *J. Mater Sci.* **23** (1988) 2622.
3. C. B. PONTON, R. D. RAWLINGS and P. S. ROGERS, in "Proceedings of the Conference on Special Ceramics" (The Inst. Ceramics, London, December 1986) p. 229.

4. ASTM C338-73, part 17 (1975) 287.
5. P. W. MCMILLAN, in "Glass-Ceramics" 2nd edn. (Academic Press, London, 1979).
6. W. VOGEL, in "Chemistry of Glass" (The American Ceramic Society, Ohio, 1985) p. 22.
7. F. BASHFORTH and J. C. ADAMS, in "An attempt to Test Theories of Capillarity" (Cambridge University Press, Cambridge, 1883).
8. C. T. MOYNIHAN, A. J. EASTEAL and J. WILDER, *J. Phys. Chem.* **78** (1974) 2673.
9. M. CAMPBELL, Internal Report, Imperial College (1983).
10. A. MAROTTA, S. SAIELLO and A. BURI, *J. Non-cryst. Solids* **57** (1983) 473.
11. H. KISSINGER, *Anal. Chem.* **29** (1957) 1702.
12. J. A. AUGIS and J. D. BENNETT, *J. Thermal Anal.* **13** (2) (1978) 283.
13. R. J. KIRKPATRICK, *Amer. J. Sci.* **274** (1974) 215.
14. L. KLEIN and D. R. UHLMANN, *J. Geophys. Res.* **79** (1974) 4869.
15. L. R. BARRETT and A. G. THOMAS, *J. Soc. Glass. Technol.* **43** (1959) 179.
16. M. L. WILLIAMS, R. F. LANDEL and J. D. FERRY, *J. Amer. Chem. Soc.* **77** (1955) 3701.
17. G. ADAM and J. H. GIBBS, *J. Chem. Phys.* **43** (1965) 139.
18. I. GUTZOW, *Contemp. Phys.* **21** (1980) 121.
19. J. WILLIAMSON, A. J. TIPPLE and P. S. ROGERS, *J. Iron and Steel Inst.* **206** (1968) 898.
20. S. CARTER, Internal report, Imperial College (1986).
21. W. D. KINGERY, H. K. BOWEN and D. R. UHLMANN, in "Introduction to Ceramics" (Wiley, Chichester, 1976) p. 604.
22. P. S. TURNER, *J. Res. NBS* **37** (1946) 239.
23. R. S. CARMICHAEL, in "Handbook of Physical Properties of Rocks, Vol. III" (CRC Press, Cleveland, 1984) p. 102.
24. D. G. HOLLOWAY, in "The Physical Properties of Glass" (Wykeham Pub., London, 1973) p. 128.
25. G. R. RIGBY and A. T. GREEN, *Trans. Brit. Ceram. Soc.* **41** (1942) 123.
26. L. J. SHELESTAK, R. A. CHAVEZ and J. D. MACKENZIE, *J. Non-Cryst. Solids* **27** (1978) 75.
27. K. MATUSITA, S. SAKKA and Y. MATSUI, *J. Mater. Sci.* **10** (1975) 961.
28. NIPPON CARBON CO. "Nicalon data sheet" (Japan, 1985).
29. "Ceramic Glossary 1984", edited by W. W. Perkins (The American Ceramic Society, 1984) p. 52.

Received 15 February
and accepted 13 June 1988